RSC Advances

ROYAL SOCIETY OF CHEMISTRY

www.rsc.org/advances

Thioester-anchored organosilatranes: Synthetic investigations and applications in Cu^{2+} ion binding and fabrication of hybrid silica nanoparticles

Gurjaspreet Singh*, Sunita Rani, Amandeep Saroa, Shally Girdhar, Jandeep Singh, Aanchal Arora, Darpandeep Aulakh, Mario Wriedt*

Abstract

This work presents the design, synthesis, UV-Vis absorption properties and Cu^{2+} ion binding of the organo-silicon complexes (**3a**-**h**) with different coordination abilities that are derived from mercaptopropylsilatrane (MPS) and respective heteroaromatic carboxylic acids (**1a**-**h**). The prepared thioester based organosilatranes (ThE-OS) have been meticulously characterized by a series of characterization techniques such as elemental analyses, FT-IR, NMR (^{1}H, ^{13}C), LC-MS, and structure of **3e** was unambiguously determined by X-ray single crystal analyses. All the compounds have shown judicious absorption enhancement in the intensity as well as λ_{max} values on binding with Cu^{2+} ions compared to other surveyed metal ions. In addition, it is for the first time that the hybrid silica nanoparticles (H-SiNPs) bearing thioester linkage in the silica framework are reported. The synthesis was achieved conveniently by an in situ co-condensation reaction of tetraethyl orthosilicate (TEOS) with the corresponding ThE-OS. The derivatization of silica is confirmed by FT-IR, ^{13}C and ^{29}Si solid state CP-MAS NMR, UV-Vis, TEM, XRD, TGA and EDX techniques. Furthermore, the H-SiNPs have exhibited greater affinity towards Cu^{2+} ions than the parent ThE-OS.

Keywords: Organosilatranes, Silica nanoparticles, Thioester, Heterocycles, UV-Vis study, Cu^{2+} ion sensing

Introduction

The development of molecular receptors with optical characteristics that change upon binding to specific guest analyte has emerged as an inherent topic of scientific research [1]. The selective detection and quantification of vital cations such as Na^+, K^+, Mg^{2+}, Cu^{2+}, Fe^{2+}, Ca^{2+} and Zn^{2+} etc., is particularly more important due to their plethora of activities in various biological and environmental processes [2]. Copper is an essential soft transition metal ion, third in abundance in human body and has a crucial role in many physiological systems such as haemoglobin biosynthesis, bone growth and nerve function regulation [3]. However, irregular levels of free Cu^{2+} ions can cause major syndromes such as Indian childhood cirrhosis, Prion disease, Menkes disease, Parkinson's disease, Wilson disease, lipid metabolism and inflammatory disorders [4]. For these reasons, much effort has been devoted to the design of selective Cu^{2+} ion chemosensors [5].

Heterocyclic aromatic systems containing nitrogen, oxygen and sulfur atoms comprise a fundamental class of organic compounds possessing myriad of applications in catalysis, pharmaceuticals, and photoluminescence [6]. Secondly, the heterocyclic ring appended chemosensors for metal ions are appealing as they provide handy scaffolds with the appropriate structural adaptability and lone pair of electrons on hetero atoms for efficient coordination [7]. Consequently, their complexes with metal ions are well-known.

Based on the 'thio' functionality, numerous chemosensing systems have been explored for the effective and fast detection of heavy transition metal ions. For instance, thioamide, thiourea, thiosemicarbazide, thiohydrazide, thioether and thio-β-enaminone based ionophores have been used as a signalling handle in a variety of probes having high selectivity and sensitivity [8-13]. These results encouraged us to develop new effective chemosensors with in-built thio functionality. We have selected thioester motif since thioesters can make up strong metal ion chelators owing to the presence of donor S atom and

–C=O group [14]. In addition, it is a key synthon in various organic transformations such as acyl transfer reactions, asymmetric additions reactions, aldol and Michael reactions etc. [15]. Thioesters are also involved in fatty acid, polyketide biosynthesis and possess stimulating roles in bactericidal, fungicidal, HIV and tumour suppression activities [16,17].

On the other hand, siliceous materials such as silica nanospheres, silica shells and molecular sieves are attracting massive interest as inorganic solid supports for organic-inorganic hybrid materials because of their excellent thermal and mechanical stability, connection feasibility with other functional groups, high surface area, biocompatibility and surface modification flexibility [18]. Organosilanes containing three alkoxy groups on silicon end have been used as the convenient silica precursors for the surface modification purpose [19]. The method, however, generally involve agglomeration and polymerization during deposition, resulting in irregular surface morphology. Silatranes are triethanolamine-capped trialkoxysilanes, where silicon is locked into a penta coordinate position, and have an edge over alkoxysilanes in terms of hydrolytic and environmental stability, purification ease, and fewer polymerization chances [20]. Subsequently, several advanced materials have also been formulated with the use of silatranyl group as a superior substrate to link organic molecules to the metal oxide surface. The whole process occurs *via* nucleophilic attack by the surface hydroxyl groups on the silicon site forming siloxyl bonds on the surface [21]. Such hybrid materials have found promising activities in many fields including heterogeneous catalysis, solar photovoltaic cells, DNA imaging, and are recently involved in the active field of chemosensing [22,23].

Keeping the above perspectives in mind and taking forward our research interests that include the synthesis and application of silatrane based molecular receptors for selective analyte sensing [24], we herein report systematic investigations of a family of organosilatranes tailored with topologically interesting thioester linkage conjugated to

various heterocyclic rings and their applicability as Cu^{2+} ion sensors. Moreover, by embedding one of the derivatized silatranyl modules onto the surface of silica nanospheres, a Cu(II)-sensing system covalently grafted onto the silica surface is constructed and then fully characterized.

Experimental

General materials and methods

The organic solvents were dried according to standard procedures [25]. Furan-2-carboxylic acid (AVERA), thiophene-2-carboxylic acid (Aldrich), pyrazine-2-carboxylic acid (Merck), picolinic acid (Aldrich), nicotinic acid (Aldrich), isonicotinic acid (Aldrich), 2,6-pyridinedicarboxylic acid (Spectrochem), 2,3-pyridinedicarboxylic acid (Spectrochem), N,N-carbonyldiimidazole (Aldrich), 3-mercaptopropyltrimethoxysilane (Aldrich), TEOS (Aldrich) and triethanolamine (Merck) were used directly as received. Thionyl chloride (SDFCL) and triethylamine (Merck) were distilled prior to use. MPS was prepared by following a method already reported in the literature [26].

Melting points were measured in a Mel Temp II device using sealed capillaries. The ^{1}H and ^{13}C NMR spectra were recorded on a JEOL (AL 300 MHz) spectrometer using $CDCl_3$ as an internal reference and chemical shifts were reported relative to tetramethylsilane. Electronic spectral measurements were carried out using JASCO V-530 UV-Vis spectrophotometer. The infrared spectra were recorded as neat spectra on a Thermo Scientific NICOLET IS50 spectrophotometer. The Raman spectrum was recorded using Renishaw Raman spectrometer. Elemental analyses were obtained on a Perkin-Elmer Model 2400 CHNS elemental analyser. Mass spectral measurements (ESI source with capillary voltage, 3000V) were carried out with a WATERS, Q-TOF micro MASS spectrometer. The morphology of H-SiNPs was scrutinized using transmission electron microscopy (TEM) at 80 kV (Hitachi H-7500). X-Ray Diffraction (XRD) technique was employed using

PANalytical's X'pert PRO spectrophotometer with Cu-Kα radiation. The solid state ^{13}C and ^{29}Si cross polarization magic-angle spinning (CP-MAS) NMR spectra were recorded on a JEOL (400 MHz) solid state ready NMR spectrometer. The Energy Dispersive X-ray (EDX) analysis was performed on JEOL JSM-6610 LV using voltage of 15 kV. Thermogravimetric (TG) analyses were carried out on SDT Q 600 V20.9 Build 20 TGA instrument. The sample was loaded in alumina pans and ramped at 10 °C/ min from 25-1000 °C in dry air at 60 ml/min.

Single crystal X-ray diffraction measurements

Data collections were performed on single crystals coated with Paratone-N oil and mounted on Kapton loops. Single crystal X-ray data of all compounds were collected on a Bruker Kappa Apex II X-ray diffractometer outfitted with a Mo X-ray source (sealed tube, λ = 0.71073 Å) and an APEX II CCD detector equipped with an Oxford Cryosystems Desktop Cooler low temperature device. The APEX-II software suite was used for data collection, cell refinement, and reduction [27]. Absorption corrections were applied using SADABS [28]. Space group assignments were determined by examination of systematic absences, *E*-statistics, and successive refinement of the structures. Structure solutions were performed with direct methods using SHELXT-2014, and structure refinements were performed by least-squares refinements against $|F|^2$ followed by difference Fourier synthesis using SHELXL-2014 [29-31]. All non-hydrogen atoms were refined with anisotropic displacement parameters. The C-H atoms were positioned with idealized geometry and were refined with fixed isotropic displacement parameters [U_{eq}(H) = -1.2·U_{eq}(C)] using a riding model with $d_{C\text{-}H}$ = 0.95 Å (aromatic) and 0.99 Å (methylene). CCDC-1400318 contains the supplementary crystallographic data for this paper. These data can be obtained free of charge from the Cambridge Crystallographic Data Centre via www.ccdc.cam.ac.uk. The crystallographic data obtained is listed in Table T1 (supporting information).

Synthesis of ThE-OS derivatives (**3a**-**h**):

In a round bottomed flask, 1 equiv. of heteroaromatic carboxylic acid (**1a**-**h**) and 1.20 equiv. of N,N'-Carbonyldiimidazole (CDI) were added in THF (30 ml) at room temperature. CO_2 gas started releasing with increase in temperature and the reaction mixture was heated to reflux for 1 h. After cooling to room temperature, subsequent addition of MPS (1 equiv.) was carried out. The reaction mixture was heated further for 8 h and then diluted with water. The aqueous layer was extracted with ethyl acetate and the combined organic layer was washed with brine (25%) and dried over anhydrous Na_2SO_4. The mixture was concentrated in *vacuo* to give a crude material that was then purified by silica gel column chromatography (ethyl acetate:hexane, 1:2) to afford pure organosilatranyl derivatives.

Spectroscopic data for compounds (3a-h)

*S-3-(2,8,9-trioxa-5-aza-1-sila-bicyclo[3.3.3]undecan-1-yl)propyl furan-2-carbothioate (**3a**)*

The reactants used were as follows: **1a** (0.50 g, 4.46 mmol), CDI (0.72 g, 5.36 mmol), MPS (1.11 g, 4.46 mmol). Yield: 79%; m.p. = 169-171 °C; empirical formula: $C_{14}H_{21}NO_5SSi$: anal. calcd: C, 48.9; H, 6.1; N, 4.1; S, 9.3; found: C, 48.8; H, 6.0; N, 4.2; S, 9.2. IR (Neat, cm^{-1}): 1642 (*v* C═O), 1098 (*v* Si–O), 693 (*v* C–S), 581 (*v* N→Si). ^1H NMR (300 MHz, $CDCl_3$, 25 °C): δ = 0.35 (m, 2H, $SiCH_2$), 1.58 (m, 2H, CCH_2C), 2.65 (t, 6H, NCH_2, J = 5.7 Hz), 2.90 (t, 2H, CH_2S, J = 7.3 Hz), 3.59 (t, 6H, OCH_2, J = 5.7 Hz), 6.37 (t, 1H, H^3, J = 4.5 Hz), 6.98 (d, 1H, H^2, J = 4.6 Hz), 7.41 (s, 1H, H^4). ^{13}C NMR (75 MHz, $CDCl_3$, 25 °C): δ = 9.37 ($SiCH_2$), 15.84 ($C\mathbf{C}H_2C$), 31.57 (CH_2S), 50.98 (NCH_2), 57.56 (OCH_2), 111.92 (C^3), 121.01 (C^2), 145.47 (C^4), 151.48 (C^1), 180.86 (C═O). MS *m/z* (relative abundance (%), assignment): 366 (100, $(M+Na)^+$).

*S-3-(2,8,9-trioxa-5-aza-1-sila-bicyclo[3.3.3]undecan-1-yl)propyl thiophene-2-carbothioate (**3b**)*

The reactants used were as follows: **1b** (0.50 g, 3.90 mmol), CDI (0.76 g, 4.69 mmol), MPS (0.97 g, 3.90 mmol).Yield: 73%; m.p. = 169-171 °C; empirical formula: $C_{14}H_{21}NO_4S_2Si$: anal. calcd: C, 46.8; H, 5.9; N, 3.9; S,17.8; found: C, 46.6; H, 5.7; N, 3.8; S, 17.5. IR (Neat, cm^{-1}): 1641 (*v* C═O), 1096 (*v* Si–O), 692 (*v* C–S), 585 (*v* N→Si). ^{1}H NMR (300 MHz, $CDCl_3$, 25 °C): δ = 0.39 (m, 2H, $SiCH_2$), 1.64 (m, 2H, CCH_2C), 2.69 (t, 6H, NCH_2, *J* = 5.7 Hz), 2.97 (t, 2H, CH_2S, *J* = 7.3 Hz), 3.63 (t, 6H, OCH_2, *J* = 5.7 Hz), 7.00 (t, 1H, H^3, *J* = 4.5 Hz), 7.49 (d, 1H, H^2, *J* = 5.0 Hz), 7.66 (d, 1H, H^4, *J* = 3.7 Hz). ^{13}C NMR (75 MHz, $CDCl_3$, 25 °C): δ = 9.38 ($SiCH_2$), 15.80 ($C\mathbf{C}H_2C$), 36.61 (CH_2S), 50.84 (NCH_2), 57.40 (OCH_2), 127.57 (C^3), 130.32 (C^2), 131.66 (C^4), 142.83 (C^1), 183.82 (C═O). MS *m/z* (relative abundance (%), assignment): 398 (100, $(M+K)^+$).

*S-3-(2,8,9-trioxa-5-aza-1-sila-bicyclo[3.3.3]undecan-1-yl)propyl pyridine-2-carbothioate (**3c**)*

The reactants used were as follows: **1c** (0.50 g, 4.06 mmol), CDI (0.79 g, 4.87 mmol), MPS (1.01 g, 4.06 mmol).Yield: 80%; m.p. = 160-162 °C; empirical formula: $C_{15}H_{22}N_2O_4SSi$: anal. calcd: C, 50.8; H, 6.2; N, 7.9; S, 9.0; found: C, 50.5; H, 6.3; N, 7.6; S, 8.8. IR (Neat, cm^{-1}): 1650 (*v* C═O), 1090 (*v* Si–O), 665 (*v* C–S), 576 (*v* N→Si). ^{1}H NMR (300 MHz, $CDCl_3$, 25 °C): δ = 0.46 (m, 2H, $SiCH_2$), 1.68 (m, 2H, CCH_2C), 2.73 (t, 6H, NCH_2, *J* = 5.8 Hz), 3.02 (t, 6H, CH_2S, *J* = 7.3 Hz), 3.67 (t, 6H, OCH_2, *J* = 5.7 Hz), 7.28 (m, 1H, H^4), 8.10 (m, 1H, H^3), 8.58 (d, 1H, H^2, *J* = 4.7 Hz), 8.86 (s, 1H, H^5). ^{13}C NMR (75 MHz, $CDCl_3$, 25 °C): δ = 9.87 ($SiCH_2$), 14.89 ($C\mathbf{C}H_2C$), 36.85 (CH_2S), 51.06 (NCH_2), 57.66 (OCH_2), 128.29 (C^2), 131.43 (C^4), 135.42 (C^3), 148.62 (C^5), 155.50 (C^1), 190.32 (C═O). MS: *m/z* (relative abundance (%), assignment): 377 (100, $(M+Na)^+$).

*S-3-(2,8,9-trioxa-5-aza-1-sila-bicyclo[3.3.3]undecan-1-yl)propyl pyridine-3-carbothioate (**3d**)*

The reactants used were as follows: **1d** (0.50 g, 4.06 mmol), CDI (0.79 g, 4.87 mmol), MPS (1.01 g, 4.06 mmol). Yield: 82%; m.p. = 155-157 °C; empirical formula: $C_{15}H_{22}N_2O_4SSi$: anal. calcd: C, 50.8; H, 6.2; N, 7.9; S, 9.0; found: C, 50.4; H, 6.1; N, 7.7; S, 8.8. IR (Neat, cm^{-1}): 1655 (ν C═O), 1092 (ν Si–O), 687 (ν C–S), 581 (ν N→Si). ^{1}H NMR (300 MHz, $CDCl_3$, 25 °C): δ = 0.43 (m, 2H, $SiCH_2$), 1.67 (m, 2H, CCH_2C), 2.71 (t, 6H, NCH_2, J = 5.8 Hz), 3.03 (t, 2H, CH_2S, J = 7.3 Hz), 3.65 (t, 6H, OCH_2, J = 5.8 Hz), 7.29 (m, 1H, H^4), 8.11 (d, 1H, H^3, J = 5.7 Hz), 8.65 (d, 1H, H^5, J = 4.6 Hz), 9.06 (s, 1H, H^1). ^{13}C NMR (75 MHz, $CDCl_3$, 25 °C): δ = 9.51 ($SiCH_2$), 15.72 ($C\mathbf{C}H_2C$), 32.63 (CH_2S), 51.19 (NCH_2), 57.69 (OCH_2), 123.23 (C^4), 128.39 (C^2), 134.39 (C^3), 148.62 (C^5), 153.25 (C^1), 190.49 (C═O).

*S-3-(2,8,9-trioxa-5-aza-1-sila-bicyclo[3.3.3]undecan-1-yl)propyl pyridine-4-carbothioate (**3e**)*

The reactants used were as follows: **1e** (0.50 g, 4.06 mmol), CDI (0.79 g, 4.87 mmol), MPS (1.01 g, 4.06 mmol). Yield: 80%; m.p. = 155-157 °C; empirical formula: $C_{15}H_{22}N_2O_4SSi$: anal. calcd: C, 50.8; H, 6.2; N, 7.9; S, 9.0; found: C, 50.7; H, 6.1; N, 7.8; S, 9.2. IR (Neat, cm^{-1}): 1646 (ν C═O), 1094 (ν Si–O), 685 (ν C–S), 582 (ν N→Si). ^{1}H NMR (300 MHz, $CDCl_3$, 25 °C): δ = 0.38 (m, 2H, $SiCH_2$), 1.65 (m, 2H, CCH_2C), 2.70 (t, 6H, NCH_2, J = 5.4 Hz), 3.00 (t, 2H, CH_2S, J = 7.4 Hz), 3.63 (t, 6H, OCH_2, J = 5.4 Hz), 7.65 (d, 2H, $H^{2,5}$, J = 4.6 Hz), 8.65 (d, 2H, $H^{3,4}$, J = 4.6 Hz). ^{13}C NMR (75 MHz, $CDCl_3$, 25 °C): δ = 10.25 ($SiCH_2$), 15.79 ($C\mathbf{C}H_2C$), 32.60 (CH_2S), 50.86 (NCH_2), 57.37 (OCH_2), 120.12 ($C^{2,4}$), 143.52 (C^3), 150.47 ($C^{1,5}$), 190.85 (C═O).

*S-3-(2,8,9-trioxa-5-aza-1-sila-bicyclo[3.3.3]undecan-1-yl)propyl pyrazine-2-carbothioate (**3f**)*

The reactants used were as follows: **1f** (0.50 g, 4.03 mmol), CDI (0.78 g, 4.81 mmol), MPS (1.00 g, 4.01 mmol). Yield: 74%; m.p. = 169-171 °C; empirical formula: $C_{14}H_{21}N_3O_4SSi$: anal. calcd: C, 47.3; H, 5.9; N, 11.8; S, 9.0; found: C, 47.2; H, 5.8; N, 11.6; S, 8.9. IR (Neat, cm^{-1}): 1645 (*v* C═O), 1095 (*v* Si–O), 686 (*v* C–S), 580 (*v* N→Si). ^{1}H NMR (300 MHz, $CDCl_3$, 25 °C): δ = 0.39 (m, 2H, $SiCH_2$), 1.62 (m, 2H, CCH_2C), 2.73 (t, 6H, NCH_2, *J* = 5.7 Hz), 2.95 (t, 2H, CH_2S, *J* = 7.3 Hz), 3.64 (t, 6H, OCH_2, *J* = 5.7 Hz), 8.57 (m, 1H, H^4), 8.70 (t, 1H, H^3, *J* = 7.8 Hz), 9.02 (d, 1H, H^2, *J* = 4.7 Hz,). ^{13}C NMR (75 MHz, $CDCl_3$, 25 °C): δ = 9.34 ($SiCH_2$), 14.82 (CCH_2C), 36.02 (CH_2S), 51.03 (NCH_2), 57.66 (OCH_2), 143.62 (C^2), 145.73 (C^4), 147.88 ($C^{1,3}$), 193.59 (C═O). MS *m/z* (relative abundance (%), assignment): 378 (100, $(M+Na)^+$).

*S,S-bis(3-(2,8,9-trioxa-5-aza-1-sila-bicyclo[3.3.3]undecan-1-yl)propyl)pyridine-2,3 bis(carbothioate) (**3g**)*

The reactants used were as follows: **1g** (0.50 g, 2.99 mmol), CDI (1.16 g, 7.16 mmol), MPS (1.49 g, 5.98 mmol). Yield: 80%; m.p. = 170-172 °C; empirical formula: $C_{25}H_{39}N_3O_8S_2Si_2$: anal. calcd: C, 47.6, H, 6.2, N, 6.6, S, 10.2; found: C, 47.9, H, 6.8, N, 6.4, S, 10.8. IR (Neat, cm^{-1}): 1650 (*v* C═O), 1087 (*v* Si–O), 689 (*v* C–S), 585 (*v* N→Si). ^{1}H NMR (300 MHz, $CDCl_3$, 25°C): δ = 0.40 (m, 4H, $SiCH_2$), 1.60 (m, 4H, CCH_2C), 2.68 (t, 12H, NCH_2, *J* = 5.7 Hz), 3.05 (t, 4H, CH_2S, *J* = 7.2 Hz), 3.63 (t, 12H, OCH_2, *J* = 5.7 Hz), 7.57 (t, 1H, H^4, *J* = 8.1 Hz), 7.77 (d, 1H, H^5, *J* = 9.1 Hz), 8.78 (d, 1H, H^3, *J* = 9.1 Hz). ^{13}C NMR (75 MHz, $CDCl_3$, 25 °C): δ = 9.38 ($SiCH_2$), 15.42 (CCH_2C), 36.65 (CH_2S), 51.09 (NCH_2), 57.57 (OCH_2), 124.34 (C^2), 128.24 (C^4), 149.37 (C^3), 151.95 ($C^{1,5}$), 191.15 (C═O), 192.59 (C═O). MS *m/z* (relative abundance (%), assignment): 630 (100, $(M+H)^+$).

*S,S-bis(3-(2,8,9-trioxa-5-aza-1-sila-bicyclo[3.3.3]undecan-1-yl)propyl)pyridine-2,6 bis(carbothioate) (**3h**)*

The reactants used were as follows: **1h** (0.50 g, 2.99 mmol), CDI (1.16 g, 7.16 mmol), MPS (1.49 g, 5.98 mmol). Yield: 82%; m.p. = 165-167 °C; empirical formula: $C_{25}H_{39}N_3O_8S_2Si_2$: anal. calcd: C, 47.6, H, 6.2, N, 6.6, S, 10.2; found: C, 47.0, H, 6.9, N, 6.9, S, 10.8. IR (Neat, cm^{-1}): 1642 (ν C═O), 1099 (ν Si–O), 697 (ν C–S), 589 (ν N→Si). ^{1}H NMR (300 MHz, $CDCl_3$, 25°C): δ = 0.47 (m, 4H, $SiCH_2$), 1.70 (m, 4H, CCH_2C), 2.71 (t, 12H, NCH_2, J = 5.7 Hz), 2.97 (t, 4H, CH_2S, J = 7.3 Hz), 3.66 (t, 12H, OCH_2, J = 5.7 Hz), 7.87 (t, 1H, H^3, J = 9.1 Hz), 8.01 (d, 2H, $H^{2,4}$, J = 7.9 Hz). ^{13}C NMR (75 MHz, $CDCl_3$, 25 °C): δ = 10.78 ($SiCH_2$), 23.30 (CCH_2C), 37.75 (CH_2S), 51.35 (NCH_2), 57.87 (OCH_2), 123.32 (C^3), 138.62 ($C^{2,4}$), 155.82 ($C^{1,5}$), 193.23 (C═O).

Results and discussion

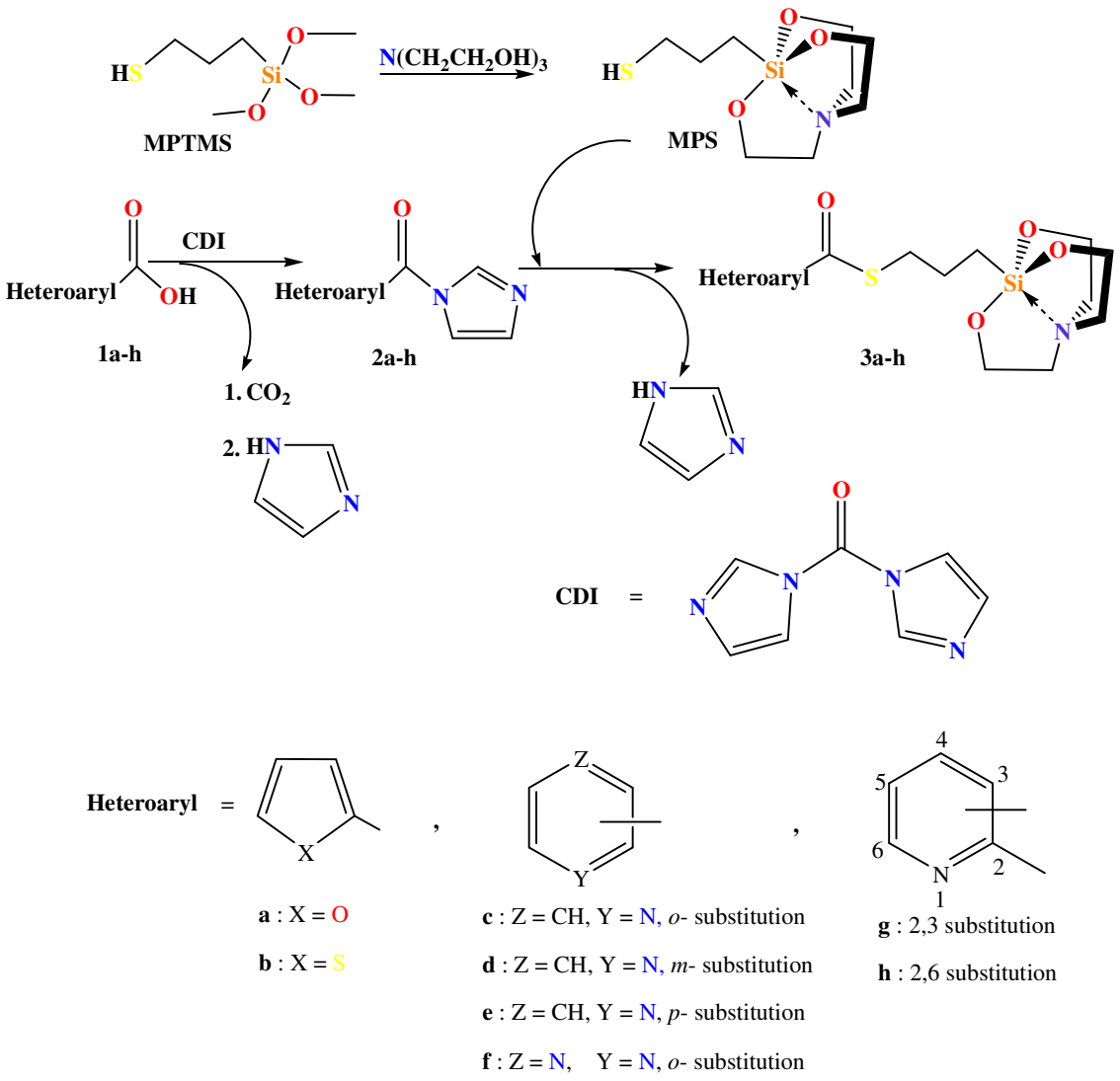

Scheme 1: Synthesis of ThE-OS derivatives (**3a**-**h**)

Synthetic approach

Overall, in our study, the synthesis of the silatranyl allied potential silica precursors (**3a**-**h**) was efficiently achieved *via* a three-step route. The first step was the formation of the MPS from 3-mercaptopropyltrimethoxysilane (MPTMS) and triethanolamine (Scheme 1). The reaction was carried out in toluene at 110 °C for 6 h and driving force here was the continuous azeotropic removal of the by-product methanol using a Dean-Stark apparatus. Simple recrystallization from chloroform afforded pure MPS with good yield.

Following this, the CDI mediated protocol of thioester synthesis was employed through a one pot reaction of MPS and carboxylic acid (Scheme 1). The reaction was performed without utilizing inert atmosphere using optimized reaction conditions (Table 1, entry 8). During the course of this reaction, imidazole and acyl carboxy substituted imidazole were formed, which combined readily to yield corresponding acylimidazole. The last step of the reaction involved the in-situ coupling of the acylimidazoles with MPS to provide ThE-OS derivatives.

Table 1 Optimization of reaction conditions for synthesis of compound **3a**

Entry	Catalyst/ coupling agent	Amount employed[a]	solvent	Reaction conditions	Reaction duration (h)	Yield (%)[b]
1	None	-	toluene	110 °C, st	8	0
2	H_2SO_4	0.2 equiv.	toluene	110 °C, st	8	30
3	$SOCl_2$	10 equiv.	$CHCl_3$	80 °C, st	5	67
4	CDI	1 equiv.	Toluene	110 °C, st	10	50
5	CDI	1.2 equiv.	Toluene	110 °C, st	8	76
6	CDI	1.3 equiv.	Toluene	110 °C, st	8	76
7	CDI	1.5 equiv.	Toluene	110 °C, st	8	76
8	**CDI**	**1.2 equiv.**	**THF**	**65 °C, st**	**8**	**79**

9	CDI	1.2 equiv.	CH_2Cl_2	40 °C, st	8	70
10	CDI	1.2 equiv.	$CHCl_3$	60 °C, st	8	72

a: the amount used is w.r.t. carboxylic acid (**3a**), b: determined by 1H NMR analysis of crude sample. The bold values specify the best optimized conditions for the reaction.

Crystallographic studies for characterization of 3e

The compound **3e** crystallizes in the monoclinic space group $P12_1/n1$ with unit cell dimensions of a = 11.5580 Å, b = 7.3752(7) Å, c = 19.4783(2) Å and β = 93.613°, Z = 4, V = 1657.1(3) Å^3, ρ (calculated) = 1.421 g·cm^{-3}. A total of 27,042 reflections were calculated, 4,117 were independent and of which 2,944 [$F_0 > 4\sigma(F_0)$] were considered observed and used in the structure analysis and refinement. All atoms are located in crystallographically independent general positions. Other crystal structure details are given in Table T1, SI. An ortep view of compound **3e** with atom labeling scheme is given in Fig. 1(A). In the asymmetric unit, the Si atom is bonded to three oxygen atoms with Si-O bond distances in the range 1.660-1.669 Å. The propyl chain with C-C-C angle of 119.03(19) ° imparts flexibility to the entire unit thereby exhibiting a lineal distance of 11.574 Å between the nitrogen atoms at the two ends.

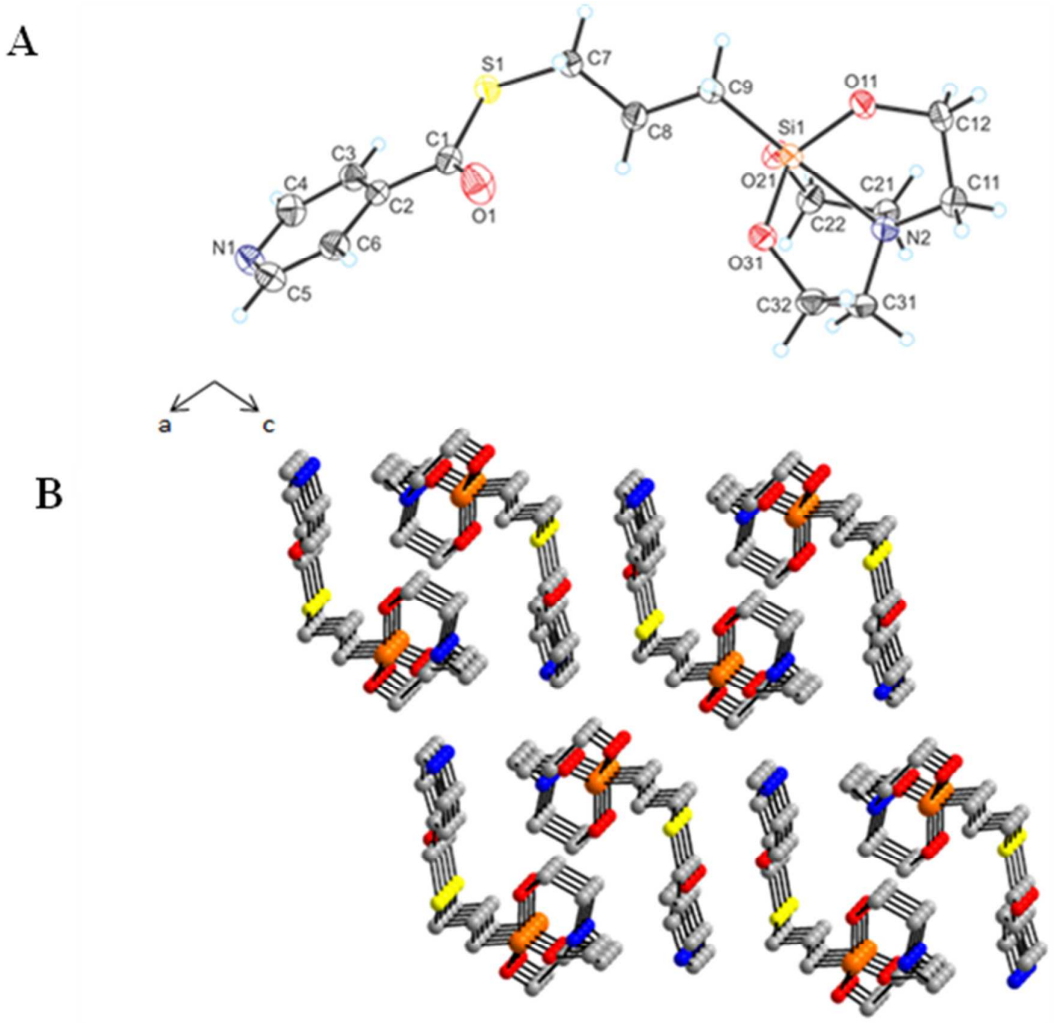

Fig. 1 (A) ORTEP showing the crystal structure of **3e** with displacement ellipsoids drawn at the 50% probability level, selected atoms are labeled. (B) 3D supramolecular coordination network with view along the crystallographic *b* axis (hydrogen atoms have been removed for clarity)

Intermolecular hydrogen bonding interactions can be observed in the crystal packing between the carbonyl oxygen O1 and C4-H4 of the pyridine ring [C4-H4···O1, 2.404 Å; angle C4-H4-O1, 141.53°] (Fig. 1(B)). In addition similar hydrogen bonding interactions can be observed for C5-H5 of the pyridine ring with O21 attached to the Si atom [C5-H5···O21,

2.460 Å; angle C5-H5-O21, 138.36°]. These intermolecular hydrogen bonding interactions give rise to the polymeric chains along the crystallographic *b* axis.

UV-Vis absorption studies

Choice of solvent system

Analysing the response of a chemoreceptor in different solvent systems is primarily important as changes in the environment may reorient corresponding energy levels, which can significantly affect the position, shape and intensity of the absorption bands. For instance, **3a** has shown doublet type absorption bands with two λ_{max} values in CH_3CN (Fig. S1, supporting information). However, a broad peak has been observed in the CH_3OH solvent system. Similar behaviour is shown by other derivatives as well. This means two absorption bands of each receptor merge to make a broad band in CH_3OH due to the H-bonded solute-solvent complex formation, replacing the fine structure present in CH_3CN [32]. Additionally, CH_3OH as a donor solvent may interact with the surveyed metal ions during titrations. To avoid these interactions, all the spectra were recorded in CH_3CN.

ThE-OS derivatives exhibit major absorption bands in the region of 215-295 cm^{-1}, which are ascribed to the π-π* electronic transitions in these conjugate systems and the features of the absorption peaks are presented in Table 2.

Table 2 Observed UV-Vis absorption parameters for chemoreceptors **3a**-**h** and their metal complexes

ThE-OS derivative	**λ_{max} (nm)**	**$\varepsilon_{max} \times 10^4$ ($Lmol^{-1}cm^{-1}$)**	**λ_{max} after saturated with Cu^{2+}**	**Stoichiometry of complexation (ThE-OS:Cu^{2+})**	**Association constant**
3a	216, 256	10.70, 11.40	261	1:1	1.63×10^5 M^{-1}

3b	250, 292	10.52, 11.33	-	1:1	3.81×10^5 M^{-1}
3c	216, 272	15.57, 10.26	302	1:1	3.61×10^5 M^{-1}
3d	223, 271	10.80, 10.27	300	1:1	3.15×10^5 M^{-1}
3e	225, 272	7.86, 7.94	296	1:2	3.82×10^3 $M^{-1/2}$
3f	222, 273	10.05, 9.97	283	1:1	2.64×10^5 M^{-1}
3g	251, 291	10.11, 11.61	318	1:1	3.73×10^5 M^{-1}
3h	240, 286	10.52, 10.80	292	1:1	4.93×10^5 M^{-1}
H-SiNPs	230, 283	-	297	1:1	5.24×10^5 M^{-1}

It is observed that the different heterocyclic rings have significantly affected the absorption maxima values. Considering the five-membered heterocycles used in this manuscript, **3a** containing a furan ring conjugated with thioester group has two absorption bands at λ_{max} values of 215 nm and 284 nm. As compared to **3a**, the bathochromic shift in compound **3b** featuring a thiophene unit (Fig. S2) emphasizes the effect of substitution of O by S atom along with a better degree of conjugation [33].

Switching from five- to six-member heterocyclic ring linker (**3c**-**e**), similar bathochromic changes are observed (Table 2). These shifts are a direct consequence of the extension of π-conjugation length [24(a)]. On the other hand, the positional isomeric effect in compounds **3c**-**e** is inoperative to alter the absorption behaviour as shown in Fig. S3. Similarly, the electron withdrawing inductive effect of extra N atom in the pyrazine ring **(3f)** fails to make any considerable change in the absorption pattern as compared to compounds **3c**-**e** (Fig. S3)**.** The di-silatranyl substituted pyridine ring derivatives (**3g**-**h**) have acquired higher λ_{max} values than the mono ones, owing to the additional thioester group conjugation (Fig. S4).

Recognition studies involving cations

All the recognition studies were performed at 25 °C and before recording any spectrum, adequate time was given to ensure the uniformity of the solution. The sensing abilities of all compounds were examined by adding various cations (20 equiv.) such as Na^+, K^+, Mg^{2+}, Al^{3+}, Ni^{2+}, Cu^{2+}, Co^{2+}, Fe^{2+}, Zn^{2+}, Cd^{2+}, Hg^{2+} to CH_3CN solution of each receptor (1 μM). The addition of all cations except Cu^{2+} caused only nominal spectrum changes in any of the compound (Figs. S5-S12).

UV-Vis titration experiments with the receptors **3a**-**h** and copper ions showed, in most of the cases, a similar behaviour, namely the addition perturbed the absorption bands by altering both intensity as well as wavelength maxima. The general trend observed is as follows: Adding copper ions to the CH_3CN solutions of receptors resulted in the margining of two bands to a single band. A significant red shift was simultaneously observed in these spectra, which may be attributed to the increase in conjugation and consequently decrease in the π-π* transition energy difference [34]. The intensity of this red-shifted band increased with increasing concentration of Cu^{2+} ions and eventually reached to limiting value when the addition continued (nearly 2 equiv. of Cu^{2+} ions for **3h**, 4 equiv. for **3b**, **3c**, **3d**, **3g** and 10 equiv. for **3a**, **3e** and **3f**). The relative intensity and the position of the red-shifted band with addition of Cu^{2+} ions mainly depend on the receptor used. Since the absorption changes occurred in the UV region (below 400 nm), any colour change was not observed throughout the titrations [35].

Mode of binding

The thioester group is a fascinating ambidentate functional group as it possesses two different types of binding sites: the soft S donor site and the π electron donor, –C=O group. Consequently, two linkage isomers are possible for the corresponding metal complexes formed (Scheme 2).

Scheme 2: Possible linkage isomers for thioester-metal complexes

To date, research on exploring the binding attribute of thioester moiety has been scarce [14]. Howbeit, there are a few reports on the crystal structures of metal complexes with oxo-esters, where the coordination to a transition metal center can take place either through the carbonyl O atom or through alkoxy O atom [36(a)]. The former binding mode is predominantly observed as C=O group has significant coordinative ability through its π orbitals, while the coordination from alkoxy O atom is accompanied by unfavourable steric effects, which restrict the latter's participation in the complexation. Thioesters, sulfur analogues of oxo-esters, are expected to behave similarly.

To determine the exact mode of binding, the vibrational spectroscopic tool was used. The infrared spectrum of compound **3h** reveals that the characteristic peak for C=O bond of the thioester group at 1642 cm^{-1} gets shifted to 1590 cm^{-1} in the presence of copper ions (Fig. 2). This shift can be interpreted as a result of the symmetrical coordination of the carbonyl groups of **3h** with the copper metal center. Moreover, the higher energy shift of the vibrations ascribed to the pyridine ring authenticates the participation of pyridine N in the bonding. The binding of heterocyclic unit with the copper centre was also checked by Raman spectroscopy. The Raman spectrum of **3h·Cu^{2+}**complex contains the key features associated with the pyridine ring (Fig. S13). The most intense Raman band is observed at the frequency of 1036 cm^{-1} which is higher as compared to the free pyridine ring of dipicolinic acid [36(b)]. This shift further certifies the binding of copper ions with pyridine N.

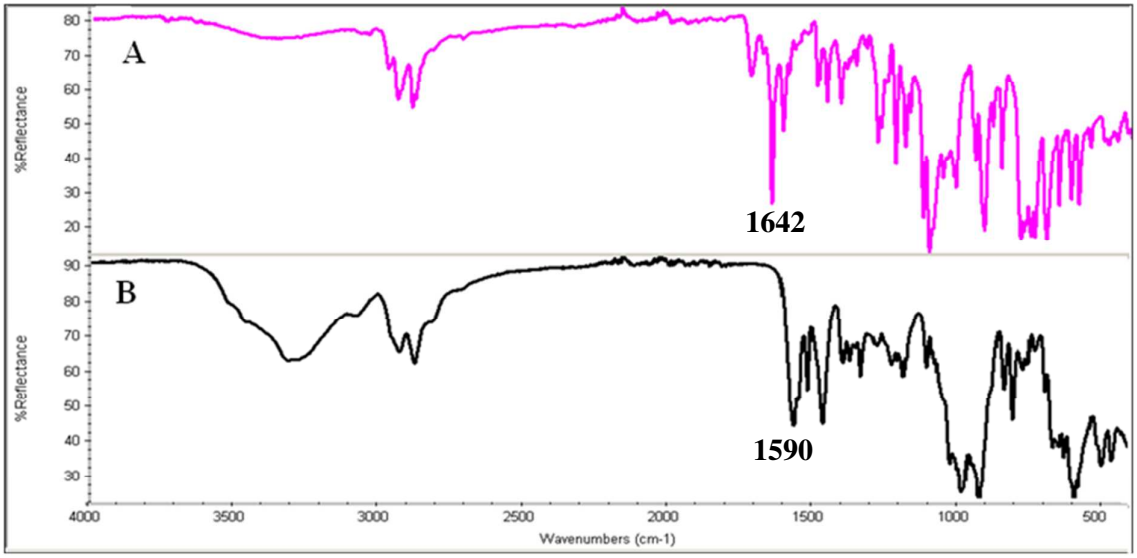

Fig. 2 IR spectra of **3h** (A) and **3h·Cu^{2+}**complex (B)

The proposed binding mode is further supported by studying the binding behaviour of compounds with Hg^{2+} ions as Hg^{2+} ions display great affinity for soft coordination center S on account of the Hard and Soft Acid and Base (HSAB) concept [37]. In our case, the receptors (except **3b**) have not shown any notable UV-Vis absorption change in the presence of Hg^{2+} ions (Figs. S5-S12). If alkthioxy S atom had been involved in the binding, some changes would have to be there in the absorption spectra, which were not observed. This reluctance of binding with Hg^{2+} ions by the receptors corroborate to the proposed binding model. However, the thiophene ring allied silatrane (**3b)** comes forth as an excellent Hg (II) binder since it is an electron-rich moiety that contains π-electrons on the C=O bond as well as lone-pair electrons on the S-atom of thiophene ring. The titration profile of receptor **3b** with Hg^{2+} ions is shown in Fig. S14.

Stoichiometry Calculations and Comparison of binding abilities

As all receptors have shown binding with copper ions, herein we endeavour to make a comparative study to estimate the strength of the interaction of copper ions with different ThE-OS derivatives. An assessment of the absorption intensity data on modified Benesi-Hildebrand (B-H) method has been exploited for the said purpose [38]. The B-H relation is

used to determine the association constant (K_a), a measure of the strength of the interaction between the ligand and the metal ions that come together to form the complex, and to determine the stoichiometry of complexation.

From the UV-Vis titration profiles, a linear regression for the plot of $[A-A_o]^{-1}$ vs. $[Cu^{2+}]^{-1}$ is obtained for all ThE-OS derivatives, except **3e**. For **3e**, as shown in Fig. S20, the B-H plot of $[A-A_o]^{-1}$ versus $[Cu^{2+}]^{-0.5}$ provides a straight line throughout the entire range of Cu^{2+} ion concentration, indicating 1:0.5 complex formation. To confirm our statement, we constructed the B-H plot for 1:1 complexation (Fig. S15). The nonlinear plot in this case again supports that the **3e**·$(Cu^{2+})_{1/2}$ complexation occurs only through 1:0.5 stoichiometry.

In the first place, on stepwise addition of Cu^{2+} ions to **3a** and **3b** solution, the absorbance intensity increased in both compounds. In **3a**, the increase was gradual and the maximum red shifted band was observed at 261 nm, when 10 equiv. Cu^{2+} ions were added (Fig. S16). While in **3b**, a plateau in the absorption graph was reached only after 4 equiv. of Cu^{2+} ions had been added (Fig. S17). It is clear from Benesi-Hildeband plots that both chemosensors **3a** and **3b** formed complexes with Cu^{2+} ions in 1:1 stoichiometry. This observation indicates that the thiophene S-atom in **3b** favoured the binding with Cu^{2+} ions, which can be explained in terms of HSAB concept. The thiophene S-atom in **3b** being a soft base is inclined to form a stable complex with Cu^{2+}, a soft acid than the furan O-atom in **3a**, which is a well-known hard acid. Further, the data in Table 2 show that the pyridine-based copper complexes are more stable than the furan-based ones. Since both N and O atoms belong to the category of hard bases, the differences in stability are accredited to the σ-donor ability of the heterocyclic donor rings (Donor number, DN = 33.1 and 6 for pyridine and furan, respectively) [39].

It is worth pointing out that with the change in the position of the thioester substituent relevant to the pyridine ring (**3c**-**e**), a significant decrease in K_a value is observed on moving

from *o*, *m* to *p* isomeric position (Table 2). The superior binding of Cu (II) by *o*- and *m*-isomers (**3c** and **3d** respectively) suggest that here the two active donor units are so oriented that their accessibility towards free copper ions is feasible, leading to better complexation (Fig. S18, S19). While with **3e**, the stoichiometry of complexation is 1:0.5 which suggests that two donor units of the receptor coordinate to the metal centre in an alternate manner (Scheme 3), due to which a stable chelate may not be formed in the solution as explicated by the lower value of K_a (Fig. S20, Table 2).

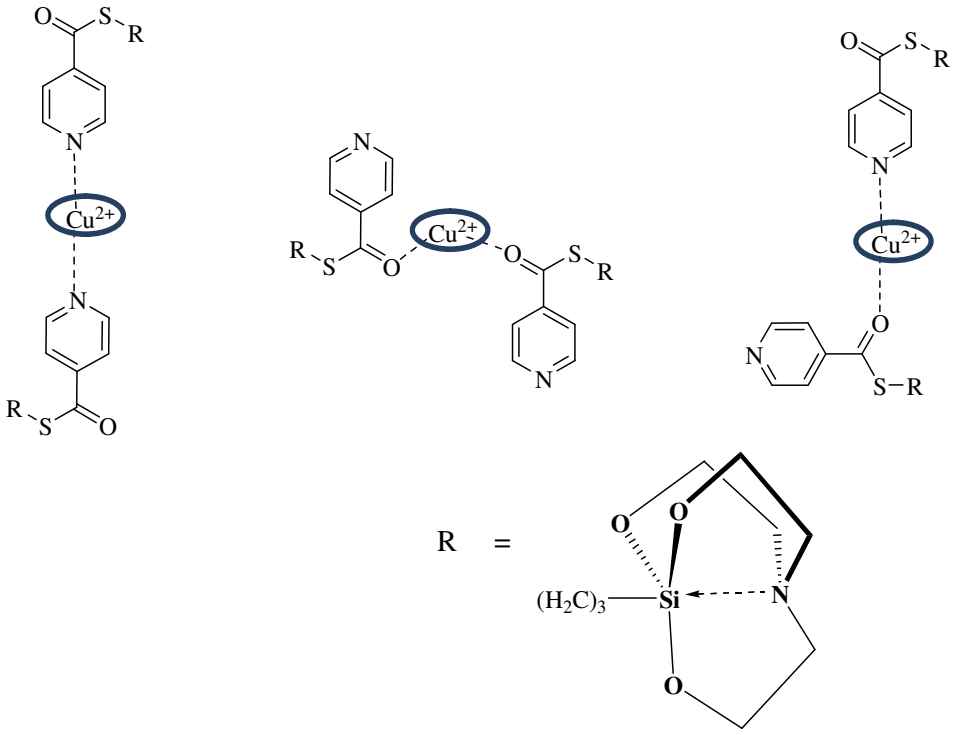

Scheme 3: Proposed binding modes of **3e** with Cu^{2+} ions

Meanwhile, the replacement of pyridine moiety to pyrazine group as part of the metal-binding unit in the organosilatranyl congener leads to decrease in the affinity for Cu^{2+}, underlying the electron withdrawing inductive effect of the second N atom of the ring and weaker binding ability (Fig. S21).

2,3 disubstituted pyridine ring derivative, **3g** behaves similar to the corresponding monosubstitud *o*-derivative, **3c** having minimal different K_a value, which hints that the second substitution at the 3-position of pyridine ring have no contribution to the bonding with copper ions (Fig. S22).

However, disubstitution at 2,6 positions improves the K_a value extensively. The presence of isosbestic point demonstrates that only one product is generated from **3h** upon binding to Cu^{2+} ions with the stoichiometry of 1:1 (Fig. 3). In fact, among the prepared compounds, **3h** comes out to be the best chemosensor for copper ions because the two thioester groups are expected to be coplanar with the central pyridine ring with their C=O bonds turned inside the cleft toward each other to construct a nice binding pocket where Cu^{2+} ions can be entrapped efficiently [40]. A comparative study is also carried out with some reported receptors bearing 'thio' functionality (Table T2) and our receptors, particularly **3h** exhibited better sensing response as shown by the higher value of K_a.

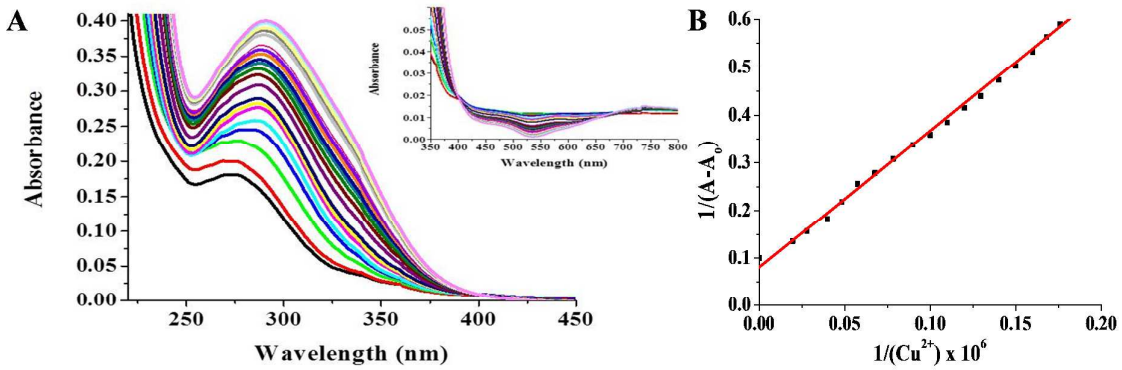

Fig. 3 (A) Family of UV–Vis spectra taken in the course of the titration of **3h** (1 μM in CH_3CN) with Cu^{2+} ions (0-2 equiv. i.e. 0, 0.1, 0.2, 0.3, 0.4, 0.5, 0.6, 0.7, 0.8, 0.9, 1.0, 1.1, 1.2, 1.3, 1.4, 1.5, 1.6, 1.7, 1.8, 1.9, 2.0). Inset shows the isosbestic point; (B) B-H plot for 1:1 complexation between **3h** and Cu^{2+} at 292 nm (R = 0.9975)

On the basis of the above discussion, a conclusion can be drawn that the structures of the heterocyclic rings and their position with respect to thioester linkage affect not only the

maximum absorption wavelengths, but also the strength and the stoichiometry of complexation with Cu^{2+} ions, giving an insight into the different donor abilities of the heterocyclic rings.

Effect of counter anion

Experiments were performed to explore the counter ion effect on the Cu^{2+}-selective properties of the receptor **3h**. Acetate, sulfate, bromide, nitrate, and perchlorate counter anions had similar influence as compared with the chloride counter ions used in this work (Fig. S23), demonstrating that the counter ion doesn't participate in the complexation.

Synthesis of hybrid silica nanoparticles (H-SiNPs)

Once the best suitability of receptors **3h** towards Cu (II) was proved, its practical applicability was examined by anchoring it onto the silica surface. The synthesis was achieved by a two-step sequence using a modified Stöber method (Scheme 4) [41].

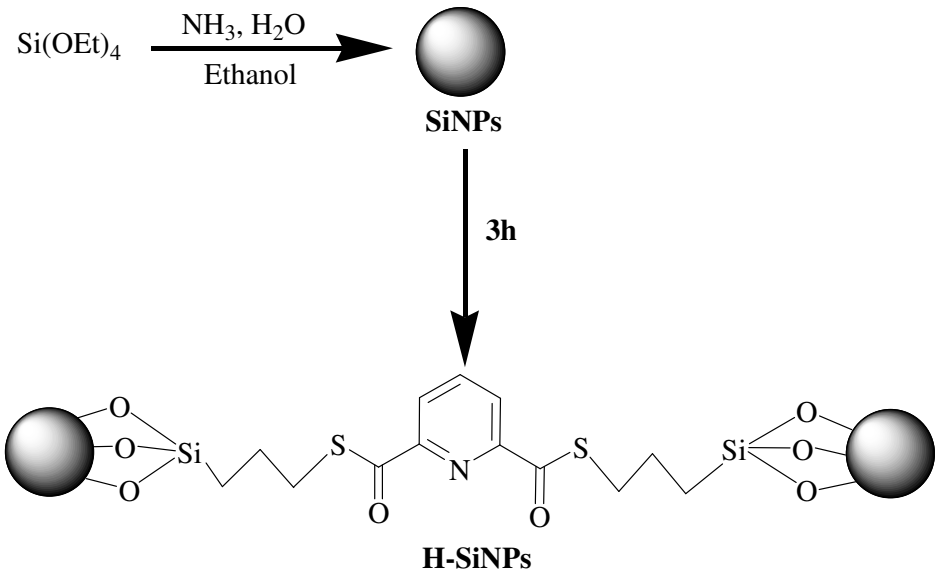

Scheme 4: Modification of silica surfaces with silatrane **3h**

The H-SiNPs were prepared by stirring 2.00 ml of TEOS and 6.00 ml of aqueous (25%) ammonia solution in 45 ml of ethanol at room temperature. After a time period of 1 h, the solution turned milky indicating the formation of silica nanoparticles (SiNPs). Further, to

carry out the desired coating on these particles, **3h** (0.629 g, 1.00 mmol) was added to the milky solution and stirred overnight. The resultant particles were centrifuged and washed with anhydrous ethanol (3×10 ml). The rationale behind the design of H-SiNPs lies in the fact that the chemosensor having copper-binding recognition sites is bridged between two silica units *via* the inclusion of the propyl chains as linker units which reduce the steric hindrance between the silica surfaces and the binding functionality.

Characterization of H-SiNPs

The IR spectra of ungrafted silica nanoparticles and functionalized silica nanoparticles are shown in Fig. S24. Absorption peaks at 1042 cm^{-1} corresponding to the asymmetric stretching vibration of Si-O-Si are observed. The absorption bands observed at 1630 and 3282 cm^{-1} are due to the bending and stretching vibrations of physically adsorbed water. In H-SiNPs, additional peaks at 1659, 1541, 1447 cm^{-1} are observed corresponding to C=O (thioester) and pyridine ring vibrations, respectively. This observation confirms the grafting of organic moiety onto the silica surface.

The thioester decorated organic functionalization of the silica gel was confirmed by solid state ^{13}C CP-MAS NMR spectroscopy. The ^{13}C CPMAS NMR spectrum of H-SiNPs exhibited three peaks each corresponding to propyl chain carbon atoms (Fig. 4(A)). The occurrence of peaks corresponding to pyridine ring C atoms and a well resolved peak at δ = 191.57 ppm guarantees the integrity of complete framework. The solid state ^{29}Si CP-MAS NMR spectrum contains the upfield resonance peaks attributed to native silica absorptions of siloxane ($Si(OSi)_4$) and silanol groups ($Si(OSi)_3OH$) at δ = -110.23 and -101.74 ppm, respectively (Fig. 4(B)). The peak corresponding to germinal silanol groups appeared as a small shoulder at δ = -92.46 ppm [42]. Conclusively, the peak at δ = -65.89 ppm corresponding to $C–Si(OSi)_3$ group proves the covalent linkage of organic moiety with the siloxane framework in the synthesized hybrid silica nanoparticles.

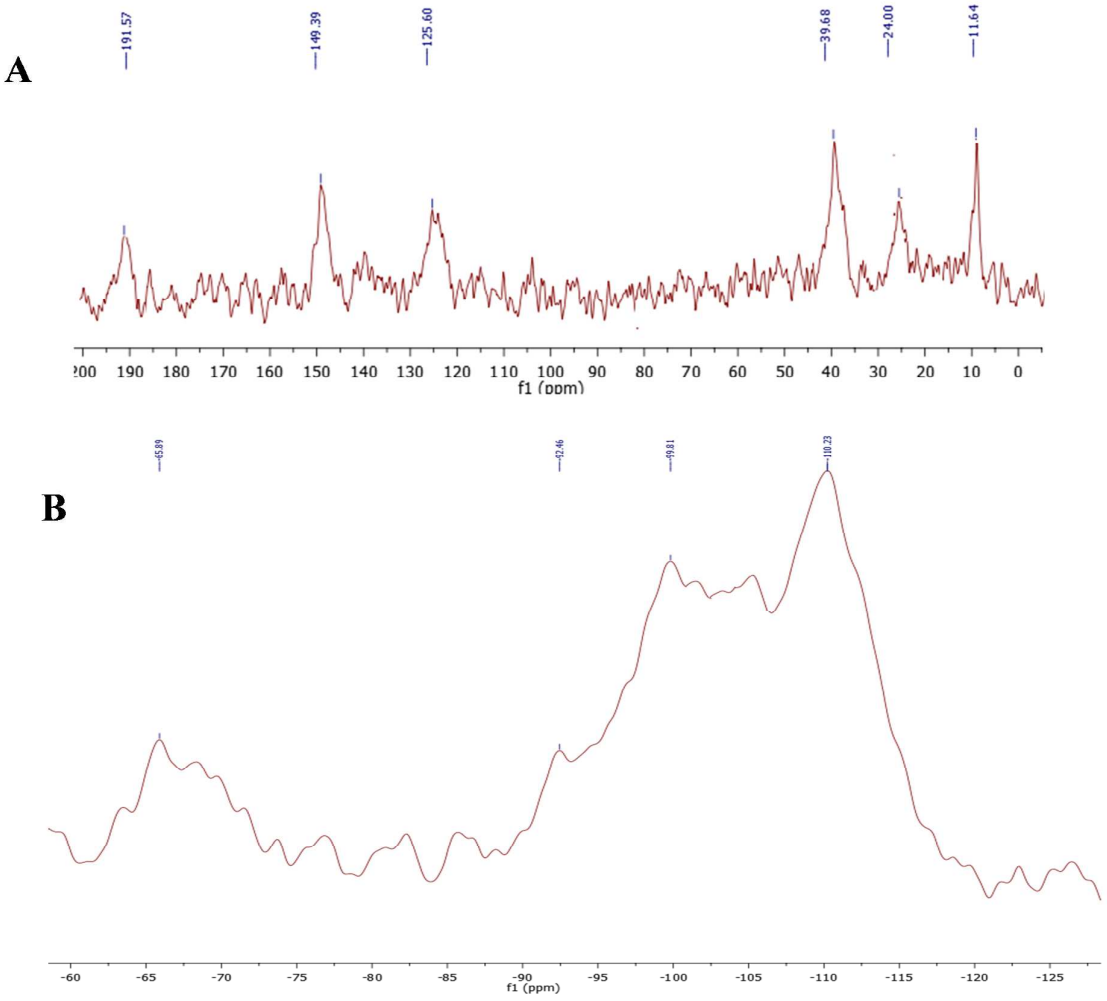

Fig. 4 ^{13}C CP-MAS NMR spectrum (A) and ^{29}Si CP-MAS NMR spectrum (B) of H-SiNPs

The TEM images of the hybrid silica nanoparticles reveal a dense layer of coating with the mean diameter of 250 nm. Few micrographs with different magnifications are presented in Fig. 5.

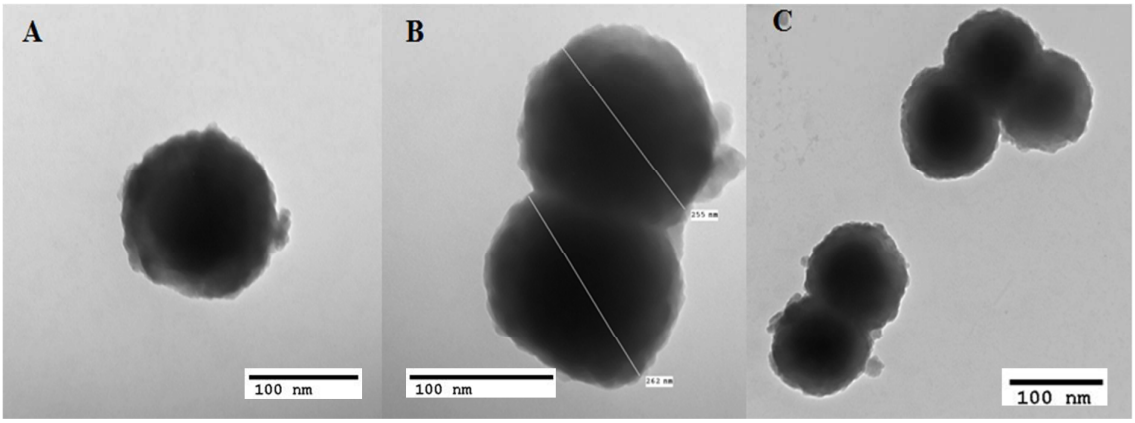

Fig. 5 Transmission Electron Micrograph (TEM) of H-SiNPs at different magnification (A-C)

As the size of unmodified silica nanoparticles lies in the range of 160-170 nm [43], this means after functionalization by the receptor **3h**, the hybrid silica nanospheres grow slightly bigger than the original silica nanospheres, confirming the coating of the organic moiety on the silica surface. The morphological homogeneity of silica nanospheres remains preserved after the surface functionalization is carried out. The silatranyl group acts as a modifier here with the release of the triethanolamine anions during the hydrolysis process which prevent the aggregation on silica surfaces leading to smoothness of coating.

The TGA curves of disilatrane **3h**, pure SiNPs and H-SiNPs were recorded to get an insight into the thermal stability and loading capacity of SiNPs. All these compounds were heated from 25 to 1000 °C under nitrogen atmosphere. The TGA curve of **3h** is a two-step profile; first step involved the weight loss due to release of ethanol from 60 to 180 °C (for ethanol calcd %: 14.60%, expt %: 13.40%) (Fig. 6). The rest of the molecule was decomposed after crossing 300 °C with the evolution of common gases leaving only silica (calcd %: 19.07%, expt %: 18.70%) at the end, which was identified after annealing to 1000 °C [44].

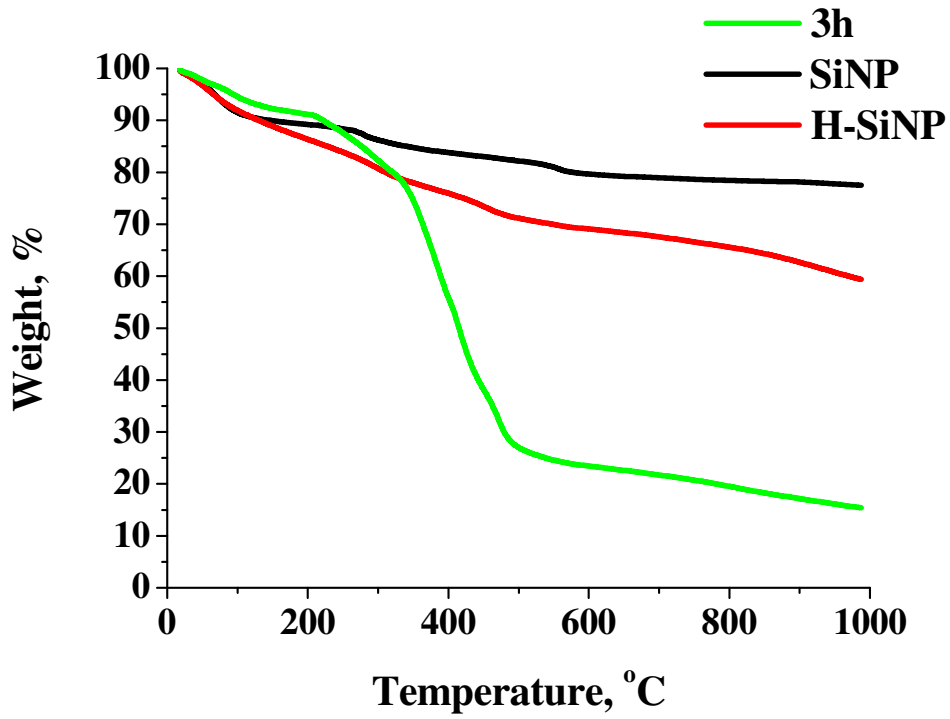

Fig. 6 Thermogravimetric curves for **3h**, SiNPs and H-SiNPs

Non-modified SiNPs showed two well defined weight loss regions; the first one, taking place in the 25–200 °C range, was due to the thermo-desorption of physically adsorbed water, indicating the presence of a hydrophilic surface. The second weight loss region from 600 °C onwards was attributed to the condensation of the free silanol groups [45]. For H-SiNPs, only 22% weight loss occurred, which proves that the remaining part of silica nanoparticles is composed of siloxane and the amount left is far more than that in **3h**. Moreover, the weight loss in H-SiNPs is greater than that observed for the SiNPs, in accordance with the loss of additional organic material affixed to the surface of H-SiNPs.

The structural features of the silica surface before and after functionalization were checked by XRD measurements. The XRD pattern for H-SiNPs shows a weak broad band at 2Θ = 21-25°, which is due to the amorphous silica shell formed (Fig. S25) [46]. The elemental composition of the H-SiNPs was investigated by EDX analysis. The characteristic peaks assigned for carbon, oxygen, nitrogen, sulfur and silicon elements are found in the

EDX spectrum as shown in Fig. 7(A), which clearly give evidence for the successful coating on the surface of the SiNPs with the framework of pyridine ring conjugated with the bis (thioester) linkage [47].

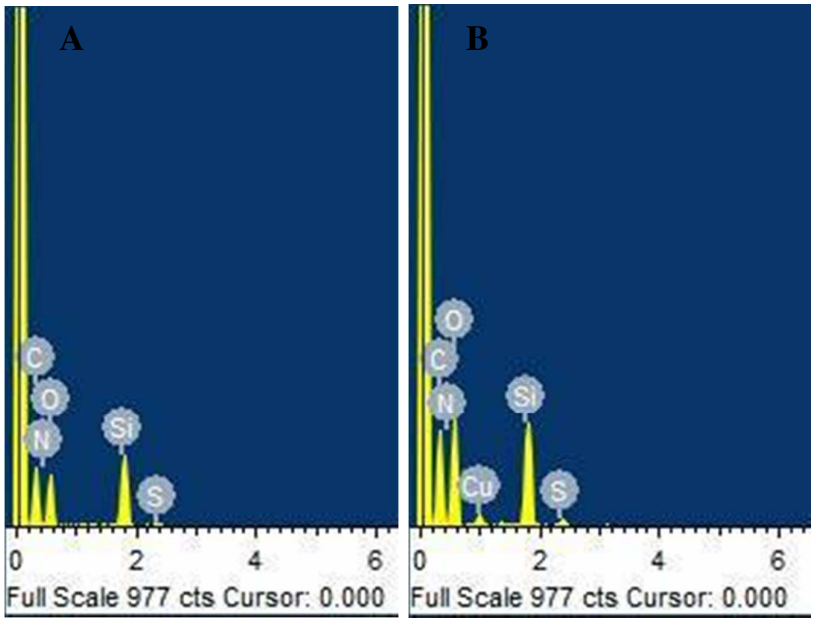

Fig. 7 Energy Dispersive X-ray (EDX) graphs of H-SiNPs (A) and Cu^{2+} loaded H-SiNPs (B)

Metal ion binding studies with H-SiNPs

The UV-Vis spectrum of H-SiNPs shows broad absorption band in the region of 270-300 nm due to π-π* electronic transitions which is comparable to those of the precursor **3h** (Fig. S26). This confirms that **3h** had been covalently anchored onto silica surface without any degradation. Further, the copper ion binding was tested with H-SiNPs and to our delight; we found that under the mastery of silica support, better results were obtained**.** The presence of one isosbestic point here also confirmed the ratio of binding of the hybrid particles with metal as 1:1 (Fig. S27). In this case, the change in absorption intensity caused by Cu^{2+} addition was more prominent as compared to change in **3h** and the value of binding constant K_a was also higher (Table 2). As the silica unit and the binding parts are covalently bonded with each other, the hybrid materials display the distinct properties together, where the stability would

be provided by the inorganic support and the organic part is required for the necessary binding sites.

Isolation of Cu^{2+}·H-SiNPs complex

We have reacted compound **3h** with $CuCl_2 \cdot 2H_2O$ in CH_3CN in 1:1 mole ratio for 4 h under continuous stirring at room temperature. Then the solvent was removed in *vacuo* to yield blue coloured solid. Further immobilization of this complex onto silica surface was carried out by the following the same procedure as used for its precursor **3h**. After similar work up, we have recorded the EDX spectrum of this material that clearly demonstrated the presence of copper ions in the hybrid structure (Fig. 7(B)). This observation supports the effective copper ion binding by H-SiNPs. A pictorial representation of pure SiNPs, H-SiNPs and Cu^{2+}·H-SiNPs have been depicted in Fig. S28. The brown colour of the H-SiNPs shows the coating of organic moiety onto the silica surface. Similarly, blue colour of Cu^{2+}·H-SiNPs signifies the presence of copper ions.

Conclusions

In nut-shell, we have synthesized a series of new organosilatranes which are tethered to a variety of heterocyclic moieties *via* thioester linker. It was found that the nature of the heterocyclic base attached to the thioester ring greatly affect the optical properties and metal ion binding properties. All these organo-silicon derivatives have the potential to be transferred into silica based organic-inorganic hybrid materials. It is shown that the pyridine ring integrated with bis(thioester) functionality was covalently attached to the silica units through flexible propyl chains. The resultant H-SiNPs have shown better binding with copper ions than the ungrafted precursor. These findings indicate that the design and synthesis of such innovative hybrid materials can be substantially important in the field of metal ion detection.

Acknowledgement

One of the authors, Sunita Rani, is grateful to the Council of Scientific and Industrial Research (CSIR), India, for providing financial support in the form of CSIR-SRF (NET) fellowship.

References

1. (a) M. Formica, V. Fusi, L. Giorgi and M. Micheloni, *Coord. Chem. Rev.*, **2012**, *256*, 170-192; (b) R. Martínej-Máñez and F. Sancenón, *Chem. Rev.*, **2003**, *103*, 4419-4476.

2. (a) B. Valeur and I. Leray, *Coord. Chem. Rev.*, **2000**, *205*, 3-40; (b) H. Y. Lin, P. Y. Cheng, C. F. Wan and A. T. Wu, *Analyst*, **2012**, *137*, 4415-4417.

3. (a) P. Kaur, D. Sareen and K. Singh, *Talanta*, **2011**, *83*, 1695-1700; (b) J. Liang, M. Qin, R. Xu, X. Gao, Y. Shen, Q. Xu, Y. Cao and W. Wang, *Chem. Commun*. **2012**, *48*, 3890-3892; (c) M. Shellaiah, Y. C. Rajan and H. C. Lin, *J. Mater. Chem*., **2012**, *22*, 8976-8987.

4. (a) J. H. Viles, *Coord Chem Rev*., **2012**, *256*, 2271-2284; (b) D. Udhayakumari, S. Velmathi, Y. Sung and S. Wu, *Sens. Actuators, B*, **2014**, *198*, 285-293; (c) P. G. Georgopoulos, A. Roy, M. J. Yonone-Lioy, R. E. Opiekun and P. J. Lioy, *J. Toxicol. Environ. Health Part B*, **2001**, *4*, 341-394.

5. J. A. Cotruvo, J. A. T. Aron, K. M. Ramos-Torres and C. J. Chang, *Chem. Soc. Rev.*, **2015**, ***DOI:*** *10.1039/C4CS00346B*

6. (a) J. Ji, T. Li and W. H. Bunnelle, *Org. Lett*., **2003**, 5, 4611-4614; (b) Z. Li, J. Xia, J. Liang, J. Yuan, G. Jin, J. Yin, G. Yu and S. H. Liu, *dyes pigments*, **2011**, *90*, 290-296.

7. A. Rajput and R. Mukherjee, *Coord Chem Rev.*, **2013***, 257,* 350-368; (b) P. Tyagi, S. Chandra, B. S. Saraswat and D. Sharma, *Spectrochim. Acta Mol. Biomol. Spectrosc.,* **2015**, *143*, 1-11; (c) D. Udhayakumari, S. Velmathi, M. S. Boobalan, P. Venkatesan and S. P. Wu, *J. Lumin.*, **2015**, *158*, 484-492.

8. Y. Guo, Y. Yan, X. Zhi, C. Yang and H. Xu, *Bioorg. Med. Chem. Lett.*, **2013**, *23*, 3382-3384.

9. M. Vonlanthen, C. M. Connelly, A. Deiters, A. Linden and N. S. Finney, *J. Org. Chem.*, **2014**, *79*, 6054-6060.

10. L. Tang, P. Zhou, Q. Zhang, Z. Huang, J. Zhao and M. Cai, *Inorg. Chem. Commun*., **2013**, *36*, 100-104.

11. H. Zheng, Z. H. Qian, L. Xu, F. F. Yuan, L. D. Lan and J. G. Xu, *Org. Lett*., **2006**, *8*, 859-861.

12. T. Chen, W. Zhu, Y. Xu, S. Zhang, X. Zhang and X. Qian, *Dalton Trans.***, 2010**, *39*, 1316-1320.

13. H. S. Kumbhar, U. N. Yadav, B. L. Gadilohar and G. S. Shankarling, *Sens. Actuators, B*, **2014**, *203*, 174–180.

14. (a) L. Feng and Z. Chen, *Sens. Actuators, B*, **2007**, *120*, 665-668; (b) C. Hou, Y. Xiong, N. Fub, C. C. Jacquot, T. C. Squier and H. Cao, *Tetrahedron Lett*., **2011**, *52*, 2692-2696.

15. (a) Y. T. Huang, S. Y. Lu, C. L. Yi and C. F. Lee, *J. Org. Chem*., **2014**, *79*, 4561-4568; (b) A. Sudalai, S. Kanagasabapathy and B. C. Benicewicz, *Org. Lett*., **2000**, *2*, 3213-3216.

16. (a) J. Staunton and K. J. Weissman, *Nat. Prod. Rep*., **2001**, *18*, 380-416; (b) D. Crich and I. Sharma, *Angew. Chem., Int. Ed*., **2009**, *48*, 2355-2358; (c) A. L. Weber, *Origins Life Evol. Biosphere*, **2005**, *35*, 421-427.

17. (a) J. L. Jios, S. I. Kirin, T. Weyhermüller, N. Metzler-Nolte and C. O. D. Védova, *J. Mol. Struct*., **2006**, *825*, 53-59.

18. (a) R. Seno and S. Kobatake, *dyes pigments*, **2015**, *114*, 166-174; (b) C. Sanchez, B. Julián, P. Belleville and M. Popall, J. Mater. Chem., **2005**, *15*, 3559-3592; (c) K. Nagase, J. Kobayashi, A. Kikuchi, Y. Akiyama, H. Kanazawa and T. Okano, *ACS Appl Mater Interfaces*, **2012**, *4*, 1998-2008; (d) Y. Li, B. Yan and J. L. Liu, *Nanoscale Res. Lett.*, **2010**, *5*, 797–804.

19. (a) A. Burns, H, Ow and U. Wiesner, *Chem. Soc. Rev*., **2006**, *35*, 1028-1042; (c) A. M. Liu, K. Hidajat, S. Kawi and D.Y. Zhao, *Chem. Commun*., **2000**, 1145-1146.

20. (a) S. P. Narula, R. Shankar, M. Kumar, R. K. Chadha and C. Janaik, *Inorg. Chem*. **1997**, *36*, 1268–1273; (b) G. Chung, O. Kwon and Y. Kwon, *Inorg. Chem.* **1999**, *38*, 197–200.

21. B. J. Brennan, M. J. L. Portole´s, P. A. Liddell, T. A. Moore, A. L. Moore and D. Gust, *Phys. Chem. Chem. Phys.,* **2013**, *15*, 16605-16614.

22. (a) S. Cabrera, H. J. El, C. Guillem, J. Latorre, A. B. Porter, D. B. Porter, M. D. Marcos and P. Amoros, *Solid State Sci.*, **2000**, *2*, 405-420; (b) M. Comes, E. Aznar, M. Moragues, M. D. Marcos, R. Martinez-Manez, F. Sancenon, J. Soto, L. A. Villaescusa, L. Gil and Pedro Amoros, *Chem. Eur. J.*, **2009**, *15*, 9024-9033; (c) B. J. Brennan, A. E. Keirstead, P. A. Liddell, S. A. Vail, T. A. Moore, A. L. Moore, D. Gust, *Nanotechnology*, **2009**, *20*, 505203.

23 (a) J. Li, K. Zhu, J. Shang, D. Wang, Z. Nie, R. Guo, C. Liu, Z. Wang, X. Li and J. Liu, *Sep. Sci. Technol*., **2012**, *47*, 1507-1513; (b) N. Thanabodeekij, E. Gulari and S. Wongkasemjit, Powder Technol. **2007**, *173*, 211-216; (c) L. S. Shlyakhtenkoa, A. A. Gall, A. Filonov, Z. Cerovac, A. Lushnikova and Y. Lyubchenko, Ultramicroscopy, **2003**, *97*, 279-287.

24. (a) G. Singh, J. Singh, S. S. Mangat, J. Singh and S. Rani, *RSC Adv*., **2015**, *5*, 12644-12654; (b) G. Singh, S. Rani, A. Saroa, Promila, A. Arora, D. C. Lazarte, *Inorg. Chim. Acta*, **2015**, *433*, 78-91; (c) G. Singh, A. Saroa, S. Girdhar, S. Rani, S. Sahoo and D. C. Lazarte, *Inorg. Chim. Acta*, **2015**, *427*, 232-239; (d) G. Singh, S. S. Mangat, H. Sharma, J. Singh, A. Arora, A. P. S. Pannu and N. Singh, *RSC Adv*., **2014**, *4*, 36834-36844; (e) G. Singh, J. Singh, S. S. Mangat and A. Arora *Tetrahedron Lett*., **2014**, *55*, 2551-2558.

25. A.I. Vogel, A Text Book of Practical Organic Chemistry, fourth ed., Longman, London, **1978**.

26. W. H. Chen, Y. T. Tseng, S. Hsieh, W.C. Liu, C. W. Hsieh, C. W. Wu, C. H. Huang, H. Y Lin, C. W. Chen, P. Y. Lin and L. K. Chau, *RSC Adv*., **2014**, *4*, 46527-46535.

27. *SAINT and APEX 2 Software for CCD Diffractometers*, Bruker AXS Inc., Madison, WI, USA, 2014.

28. G. M. Sheldrick, *SADABS, version 2014/4*, Bruker AXC Inc., Madison, WI, 2014.

29. G. M. Sheldrick, *Acta Cryst.* **2008,** *A64*, 112-122.

30. G. M. Sheldrick, *SHELXT*, University of Göttingen, Germany, 2014.

31. G. M. Sheldrick, *SHELXL*, University of Göttingen, Germany, 2014.

32. S. Dalapati, B. K. Paul, S. Jana and N. Guchhait, *Sens. Actuators, B*, **2011**, *157*, 615-620.

33. X. Zhang, H. Yu and Y. Xiao, *J. Org. Chem*. **2012**, *77*, 669-673

34. Z. Chena, Y. Wu, D. Gua and F. Gana, *Spectrochim. Acta*, Part A, **2007**, *68*, 918-926.

35. N. Kaur and P. Alreja, *Tetrahedron Lett*., **2015**, *56*, 182-186.

36. (a) P. Kapoor, A. Pathak, R. Kapoor and P. Venugopalan, *Inorg. Chem.*, **2002**, *41*, 6153-6160; (b) K. McCann, J. Laane, *J. Mol. Struct*., **2008**, *890*, 346-358.

37. E. M. Nolan and S. J. Lippard, *Chem. Rev.* **2008,** *108,* 3443-3480.

38. H. A. Benesi and J. H. Hildebrand, *J. Am. Chem. Soc*., **1949**, *71*, 2703-2707.

39. F. Piccinelli, M. Bettinelli, A. Melchior, C. Graziolib and M. Tolazzi, *Dalton Trans*., **2015**, *44*, 182-192.

40. A. Dorazco-González, M. F. Alamo, C. Godoy-Alcántar, H. Höpflc and A. K. Yatsimirsky, *RSC Adv*., **2014**, *4*, 455-466.

41. I. A. M. Ibrahim, A. A. F. Zikry and M. A. Sharaf, *J. Am. Sci*., **2010**, *6*, 985-989.

42. (a) R.K. Sharma, S. Gulati and A. Pandey, *Inorg. Chim. Acta*, **2013**, *397*, 21-31; (b) S. Omar and R. Abu-Reziq, *J. Phys. Chem. C*, **2014**, *118*, 30045-30056.

43. R. Mutneja, R. Singh, V. Kaur, J. Wagler and E. Kroke, *dyes pigments* **2014**, *108*, 41-49

44. G. Singh, A. Arora, S. S. Mangat, J. Singh, S. Chaudhary, N. Kaur and D. Choquesillo-Lazarte, *J. Mol. Struct*., **2015**, *1079*, 173-181

45. G. Sánchez, D. Curiel, I. Ratera, A. Tárraga, J. Veciana and P. Molina, *Dalton Trans*., **2013**, *42*, 6318-6326

46. J. L. Liu, S. Xu and B. Yan, *Colloids Surf. A*, **2011**, *373*, 116-123.

47. E. Kim, H. J. Kim, D. R. Bae, S. J. Lee, E. J. Cho, M. R. Seo, J. S. Kim and J. H. Jung, *New J. Chem*., **2008**, *32*, 1003-1007.